



Analytical and experimental investigations on the fracture behavior of hybrid fiber reinforced concrete



Tarek Almusallam, S.M. Ibrahim, Yousef Al-Salloum, Aref Abadel, Husain Abbas*

MMB Chair of Research and Studies in Strengthening and Rehabilitation of Structures, Department of Civil Engineering, College of Engineering, King Saud University, Riyadh 11421, Saudi Arabia

ARTICLE INFO

Article history:

Received 9 February 2016

Received in revised form

16 June 2016

Accepted 1 October 2016

Available online 5 October 2016

Keywords:

Fibers

Concrete

Fracture

Tensile strength

Inverse analysis

Reinforcing index

ABSTRACT

In the present study, Mode-I fracture tests of hybrid fiber reinforced concrete (HFRC) composite beams were conducted and the fracture properties and other post peak strength characteristics of the HFRC composites were evaluated and analyzed. The HFRC composite was produced using three types of fibers namely steel, Kevlar and polypropylene. A total of 27 HFRC composite beam specimens were cast and tested using the RILEM recommended three point bending test. The main variables were the fiber volume content and combinations of different fibers. The load versus crack mouth opening displacement (CMOD) curves of HFRC composite beams were obtained. Inverse analysis was carried out to determine the tensile strength and crack opening relationship. Analytical models based on comprehensive reinforcing index were developed for determining the influence of the fibers on fracture energy, flexural tensile strength, equivalent tensile strengths and residual tensile strengths of HFRC composites. Based on the experimental results and inverse analysis, a model for predicting the tensile softening diagram of HFRC composite mixes was also developed. The analytical models show conformity with the experimental results.

© 2016 Elsevier Ltd. All rights reserved.

1. Introduction

After the success of steel fiber reinforced concrete (SFRC) composite in improving the tensile properties of concrete [1,2], this concept was extended to the production of hybrid fiber reinforced concrete (HFRC) composites by mixing different types of fibers. Due to the contribution of fibers, HFRC composites show an increase in the strength (especially the tensile strength) and a strain softening behavior for significant strain values. Compared to the plain concrete, the increase in the toughness of the HFRC composite is mainly due to the fiber bridging and good bond behavior. The major role played by the fibers in the HFRC composites occurs in the post-cracking zone wherein redistribution of the load between the matrix and the fibers occurs [3–5]. There is a wide application of HFRC composites in precast concrete elements with reduced sections, improved impact resistance and crack control. Due to the hybridization, the HFRC composites show the synergistic effect i.e. two or more than two types of fibers contributing towards the mechanical properties both individually and as a group [5]. In

recent studies, hybrid fiber reinforced concrete (HFRC) composites were produced by mixing different types of fibers which were found to be quite effective in resisting impact loads [6–10].

Fracture studies and the post-cracking behavior of HFRC composites received considerable attention recently. In plain concrete, the tensile strength and other fracture parameters decline rapidly after the initiation of cracking [9]. However in the HFRC, the fibers bridge the crack openings and the post-cracking behavior is improved because of the significant increase in its tensile strength [11–13]. Amongst the various fiber combinations used in the recent studies on the mechanical characterization of HFRC, the use of two or three fiber combinations is common in most of the studies [13–27]. In the past, studies on HFRC composites were mainly conducted on typical combinations of geometrically different steel fibers [13], polyvinyl alcohol (PVA) fibers and steel fibers [14,15], polypropylene fibers with different geometrical and material properties [16], polypropylene fibers and steel fibers [2,17–25], as well as polyolefin fibers and steel fibers [26]. Some studies were also conducted on the HFRC composite produced from the combination of organic fibers with steel and synthetic fibers [5,28].

Studies in the past have also been conducted for determining the fracture parameters of fiber reinforced concrete (FRC) using

* Corresponding author.

E-mail address: abbas_husain@hotmail.com (H. Abbas).

analytical models, empirical models and nondestructive test methods. Lee and Barr [29] developed a multi-exponential model for determining the load versus CMOD curves of the SFRC. Amin et al. [30] developed a model for determining the load versus CMOD curves of SFRC. The model mainly consists of two parameters – one for the determination of the increase in the peak strength and the other for controlling the steepness of the descending branch. Using the model parameters, the authors [30] calculated the tensile stress-CMOD law and also the fracture energy of SFRC. In another study [31], the fracture energy was estimated by using the extrapolation of the load displacement curves of three point bending tests. Using the embedded discontinuity method (EDM) technique [32], a numerical study was undertaken for SFRC beams and the size dependent fracture properties as well as the post cracking behavior of SFRC beams were investigated. Li et al. [33] studied the fracture behavior and damage evaluation of PVA fiber concrete using acoustic emission techniques.

In the literature, analytical models for the tensile stress-crack opening law or the tensile softening diagram of concrete based on the inverse analysis [34–39] of the experimental results have also been used. The procedure of developing tensile softening diagram of plain concrete, using the inverse analysis procedure applied on the load–CMOD plots of the three point bending tests [34], was later extended to SFRC composites [36–38] and engineered cementitious composites (ECC) [39].

In the present study, the post-cracking behavior and the fracture properties of HFRC composites were investigated. For this purpose, a total of 27 beams with different HFRC mixes were cast. The HFRC composites were produced using different volume fractions of steel, Kevlar and polypropylene fibers in concrete mix. For determining the fracture parameters of the HFRC composite, notched beams were tested under three point loading as per the method recommended by RILEM [40]. The main variables were the fiber volume content and combination of different fibers. The load versus crack mouth opening displacement (CMOD) curves of HFRC composite beams were obtained. Inverse analysis was carried out to determine the tensile strength and crack opening relationship. Analytical models were developed in terms of the comprehensive reinforcing index for determining the influence of the fibers on fracture energy, flexural tensile strength, equivalent tensile strengths and residual tensile strengths of HFRC composites. Based on the experimental results and inverse analysis, a model for predicting the tensile softening diagram of HFRC composite mixes is also developed. The analytical models show conformity with the experimental results.

2. Research significance

The study aims to contribute to the reliable estimation of the stress-crack opening relationships of the HFRC composites that can be used for the design of HFRC structures. Since the complete load-CMOD curves of HFRC are required for carrying out the nonlinear analysis, the tension response is quantified using the models developed herein. The contributions of the study are:

- Perform experimental investigations on the post cracking behavior of HFRC composite beams tested using the RILEM recommended three point bending test [40].
- Studying the influence of different fibers used in the production of the HFRC composites on its post-cracking behavior.
- Analytical models based on comprehensive reinforcing index for the fracture properties of the HFRC composites.
- Determination of the tensile softening diagram for HFRC composites using inverse analysis.

3. Experimental program

3.1. Concrete materials and mix

The experimental studies were carried out on the high strength concrete reinforced with three types of fibers. The proportions of the constituents of the concrete matrix were same in all mixes and only the fibers proportions and contents were changed. Different HFRC composites were prepared using a constant water/cement ratio of 0.28. Two aggregate sizes of 10 mm and 5 mm were used. The superplasticizer GLI-110 and the retarder LD10 were also used. The compressive strength of concrete, f_c was determined by testing three standard cylinders (150 × 300 mm) at 28 days. The average compressive strength of plain concrete was 64.5 MPa. The composition of control mix is given in Table 1.

3.2. Fibers

The HFRC composite specimens were cast using different combinations of steel, polypropylene and Kevlar fibers. Studies on the FRC composites show that the fiber effect on the improvement of the post cracking behavior of concrete composites is quite significant when the fibers with large aspect ratio (length to diameter ratio) were used in its production [9]. The steel fibers were hooked at both ends, the polypropylene fibers were crimped and the Kevlar fibers were plain. The aspect ratios of steel, polypropylene and Kevlar fibers were 80, 57.5 and 90 respectively. The steel and polypropylene fibers were procured from the local market whereas the Kevlar fibers were prepared using needle felts of Kevlar. In order to give shape and stiffness to the Kevlar fibers during the mixing process of fresh concrete composite, the needle felts of Kevlar were epoxy wiped and then after the drying process, the fibers were cut to the required size. The physical and material parameters of fibers are presented in Table 2.


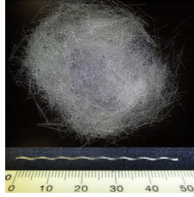

3.3. Hybrid fiber reinforced concrete (HFRC)

The HFRC composites were produced using different proportions and combinations of the steel (SF), polypropylene (PF) and Kevlar fibers (KF). Fibers with two different total volume fractions of 1.2% and 1.4% were used in the study. To alleviate the problems and difficulty of mixing and placement, the upper limit of 1.4% on the total volume fraction was kept. Eight concrete mixes (M1 to M8) of HFRC were produced by using four types of fiber combinations:

Table 1
Composition of control HFRC mix, M0.

Cement (kg/m ³)	Fine sand (kg/m ³)	Coarse aggregate (kg/m ³)		Water (w/c = 0.28) (l/m ³)	Super-plasticizer GLI-110 (l/m ³)	Retarder LD10 (l/m ³)	Compressive strength, f_c (MPa)
		Nominal maximum size = 5 mm	Nominal maximum size = 10 mm				
520	586	850	315	145	3	1.5	64.5

Table 2
Physical and mechanical properties of fibers.

	Fiber type		
	Steel (SF)	Polypropylene (PF)	Kevlar (KF)
			
Length, <i>l</i> (mm)	60	50	45
Shape	Hooked ends	Crimped	Plain
Section dimensions/equivalent diameter, <i>d</i> (mm)	0.75 ϕ (Circular)	1.0 \times 0.6 \approx 0.88 ϕ^a (Rectangular)	0.50 ϕ^a (Circular)
Specific gravity	7.85	0.90	1.45
Tensile strength (MPa)	1225	550	3220
Modulus of Elasticity (GPa)	200	4.0	131
Aspect ratio (<i>l/d</i>)	80	57.5	90

^a Approximate equivalent diameter.

(i) steel fibers alone; (ii) steel and polypropylene fibers; (iii) steel and Kevlar fibers; and (iv) all the three types of fibers. The volume fraction of steel fibers was varied from 0.7% to 1.4%. The volume fractions of polypropylene and Kevlar fibers were kept constant and taken as 0.2% and 0.3% respectively. The details of the fiber percentage used in different HFRC mixes are given in Table 3. The fibers were added to plain concrete in parts for preventing fiber balling and to ensure the homogeneity of concrete mixture. The mixing was done for about 3 min to ensure the proper distribution of fibers in the concrete mass.

The HFRC composites were divided into the following four groups [27] for the purpose of studying the influence of the addi-

Group

– 2 (M3 and M4): $\left. \begin{matrix} \text{M3: SF alone} \\ \text{M4: SF + PF} \end{matrix} \right\}$ with total fiber volume fraction = 1.4% (PF = 0.2%)

Group

– 3 (M5 and M6): $\left. \begin{matrix} \text{M5: SF + KF with total volume fraction} = 1.2\% \\ \text{M6: SF + KF with total volume fraction} = 1.4\% \end{matrix} \right\}$ KF = 0.3%

Group – 4 (M7 and M8): $\left. \begin{matrix} \text{M7: SF + PF + KF with total volume fraction} = 1.4\% \\ \text{M8: SF + PF + KF with total volume fraction} = 1.2\% \end{matrix} \right\}$ PF = 0.2%, KF = 0.3%

tion of different types of fibers on post cracking properties:

Group

– 1 (M1 and M2): $\left. \begin{matrix} \text{M1: SF alone} \\ \text{M2: SF + PF} \end{matrix} \right\}$ with total fiber volume fraction = 1.2% (PF = 0.2%)

Table 3
Fiber percentage in different HFRC composite beams.

Group	Mix/Beam	Percentage of fiber by volume (by weight)			
		Polypropylene (PF)	Steel (SF)	Kevlar (KF)	Total
Control	M0	0.0 (0.00)	0.0 (0.00)	0.0 (0.00)	0.0 (0.00)
Group-1	M1	0.0 (0.00)	1.2 (3.93)	0.0 (0.00)	1.2 (3.93)
	M2	0.2 (0.08)	1.0 (3.27)	0.0 (0.00)	1.2 (3.35)
Group-2	M3	0.0 (0.00)	1.4 (4.58)	0.0 (0.00)	1.4 (4.58)
	M4	0.2 (0.08)	1.2 (3.90)	0.0 (0.00)	1.4 (3.98)
Group-3	M5	0.0 (0.00)	0.9 (2.94)	0.3 (0.11)	1.2 (3.05)
	M6	0.0 (0.00)	1.1 (3.60)	0.3 (0.11)	1.4 (3.71)
Group-4	M7	0.2 (0.08)	0.9 (2.94)	0.3 (0.11)	1.4 (3.05)
	M8	0.2 (0.08)	0.7 (2.29)	0.3 (0.11)	1.2 (2.40)

3.4. Specimen details

Table 4 presents the test methods, prescribed by different standards [40–52], required to obtain the values of parameters for defining the post-cracking behavior of FRC. These tests mainly involve the testing of beams of different sizes in flexure except the use of circular discs in ASTM C1550 [42] for bi-axial bending response of FRC under a central point load. Although the plain concrete beams without notch are recommended by most of the standards but JCI-S-001-2003 [49] requires the testing of notched beams. The cross-section of FRC beam specimens is mostly square except for the sprayed concrete for which it is rectangular because these specimens are either cored or sawn off the panels. It may be noted from the table that the size of beam specimens of square section mainly varies from 100 to 150 mm with the span to depth ratio varying from 3 to 4. Although the notch causes fracture localization in beams due to which the recording of strain hardening is not possible but the strain hardening in FRC arises mainly due to the microcrack bridging action of short fibers (e.g. ECC) which are not used in this study. It is worth mentioning here that

Table 4
Experimental test methods for flexural strength and toughness characterization of concrete.

Test standard	Specimen size (mm)		Notch size (mm)		Loading arrangement	
	Cross section ^a , $b \times D$	Span, S	Length, L	Depth, a_0		Width, w
Plain concrete						
ASTM C 78 [45]	150×150 for $d_a \leq 50$ mm; size $\geq 3 d_a$ for $d_a > 50$ mm	3D	$S + 50$ (min.)	None	Third-point loading	
ASTM C 293–02 [44]/WSDOT [52]/AASHTO T177 [41]	150×150 for $d_a \leq 50$ mm; size $\geq 3 d_a$ for $d_a > 50$ mm	3D	$S + 50$ (min.)	None	Center-point loading	
JCI-S-001-2003 [49]	$\geq 4 d_a$	3D	$\geq 3.5D$	0.3D	5	Center-point loading
Fiber reinforced concrete						
ASTM C 1609/C 1609M–07 [43]	100×100 , 150×150 (Preferred); size $\geq 3 L_f$ (150×150 may be used for $L_f = 50–75$)	3D	$S + 50$ (min.)	None	Third-point loading	
DIN 1048 [46]	150×150	600	700	–	–	Third-point loading
EFNARC [47]	75×125	450	–	None	–	Third point loading
EN 14651 [48]	150×150 ($L_f \leq 60$; $d_a \leq 32$)	500	550–700	25	≤ 5	Center-point loading
JCI-S-002-2003 [50]	≥ 100 mm for $L_f \leq 40$ mm ≥ 150 mm for $L_f > 40$ mm	3D	$\geq 3.5D$	0.3D	5	Center-point loading
RILEM TC 162-TDF [40]	150×150 ($L_f \leq 60$; $d_a \leq 32$)	500	550	25	≤ 5	Center-point loading
UNI 11039 [51]	150×150	3D	4D	45	2	Third point loading
ASTM C 1550 [42]	$\phi 800$ disc, 75 thick; 3 pivot supports; 25 mm overhang			None		Hemispherical nose indenter

^a d_a = maximum size of aggregate; L_f = length of fibers.

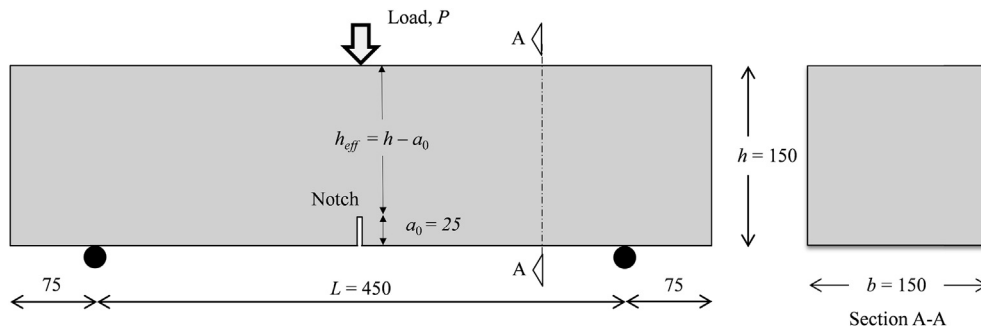


Fig. 1. Beam specimen details (All dimensions are in mm).

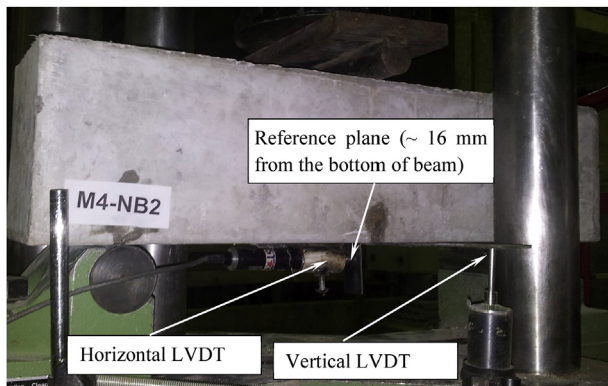


Fig. 2. Test setup for fracture testing of specimen.

the bending of beams cannot be simulated in these beam specimens but these tests may be enough for studying the fracture response of the ligament which is the prime objective in these tests. Moreover the smaller size of test specimens also helps to accommodate long fibers and at the same time keeping the weight of the beam manageable for manual handling.

For each of the eight different HFRC composites (M1 to M8) and control (M0), three standard notched beam specimens ($150 \times 150 \times 600$ mm) were cast thus making a total of 27 notched

beams. The span to depth ratio of the beams was 3 and the notch to depth ratio was 0.167. The notch was made by using 5 mm thick plastic plate at the time of casting. The top surfaces of the specimens were leveled and finished with a trowel. After casting, beam molds were kept covered under plastic sheet for one day. The beams were then demolded and cured in water for 28 days. The specimen dimensions and loading arrangement are shown in Fig. 1.

3.5. Test method

The HFRC composite beams and control beam specimens were tested for Mode-I fracture under servo-controlled electrohydraulic Zwick compression testing machine. The three point bending test, as recommended by RILEM [40], was conducted so that the high stress fracture process zones were confined at the notched section. The rate of increase of mid-span deflection of the specimen was kept constant at 0.25 mm/min. The mid-span vertical deflection was recorded by the vertical LVDT attached to the mid-span of beams as shown in Fig. 2. The CMOD was also measured simultaneously. The distance of the LVDT from the bottom face of the beam used for measuring the CMOD was kept as 16 mm. The CMOD at the beam face was calculated by using the geometrical equivalence. For HFRC composite beams, the range of vertical deflection at failure was from 5 to 8 mm. For control beams, the vertical deflection at failure was approximately 1 mm. The uniaxial compression tests were performed on cylindrical test specimens at 28 days in

Table 5
Test results.

Group	Mix/Beam specimen	Comp. strength (MPa)	Split tensile strength (MPa)	First crack load (kN)	First crack CMOD (mm)	Peak load (kN)	CMOD at peak load (mm)	Post-peak slope (up to ~10 mm) (kN/mm)
Control	M0	64.5	3.6	14.8	0.02	17.8	0.0	–
Group-1	M1	73.5	6.8	17.3	0.03	47.6	1.5	–2.0
	M2	70.0	6.4	23.8	0.02	49.2	1.7	–2.1
Group-2	M3	74.4	6.5	20.5	0.02	59.4	1.2	–2.5
	M4	71.9	6.4	21.5	0.02	60.4	1.1	–2.7
Group-3	M5	65.4	5.8	26.8	0.03	46.7	1.3	–1.9
	M6	66.0	6.3	19.7	0.02	50.8	1.1	–2.7
Group-4	M7	66.7	6.1	28.7	0.02	54.7	0.8	–2.6
	M8	65.6	6.0	25.7	0.02	46.2	1.2	–2.3

accordance with ASTM C39 [53].

4. Results and discussion

The experimental test results such as compressive strength, split tensile strength and post-peak slope of load-CMOD curve are given in Table 5. The first crack load, the maximum load and corresponding CMOD values are also reported in the table. The fracture energy and the flexural tensile strength of HFRC, calculated later,

are dependent on the strength and the corresponding strain reported in Table 5.

4.1. CMOD-deflection relationship

A relationship between the mid-span deflection, δ , and the CMOD is derived and plotted in Fig. 3. The relationship can be given by the following equation:

$$CMOD = 1.42\delta + 0.0172; \text{ (Unit: mm)} \tag{1}$$

A comparison with RILEM [40] is also shown in Fig. 3. The CMOD-deflection relationship is dependent on the geometry of the specimen and hence, remained the same for all the tested beam specimens.

4.2. Load-CMOD and load-deflection response

The load displacement and load CMOD curves for HFRC composite beams and control beams were obtained. For illustration, the salient features of the load-CMOD curves obtained for the M0 and M1 HFRC beam specimens are shown in Fig. 4. The average maximum load carrying capacity of the control beams was about 17.8 kN. For control beam specimens, no descending branch was observed and the beam failure takes place immediately after the beam reaches its maximum load carrying capacity. The response of the HFRC composite beam specimens was totally different. In comparison to the control beam, significant increase in the maximum load carrying capacity was observed in HFRC composite

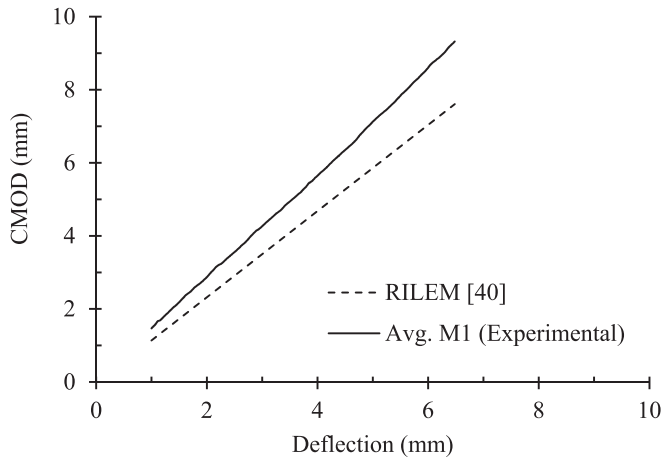


Fig. 3. CMOD-deflection relationship for M1 beams.

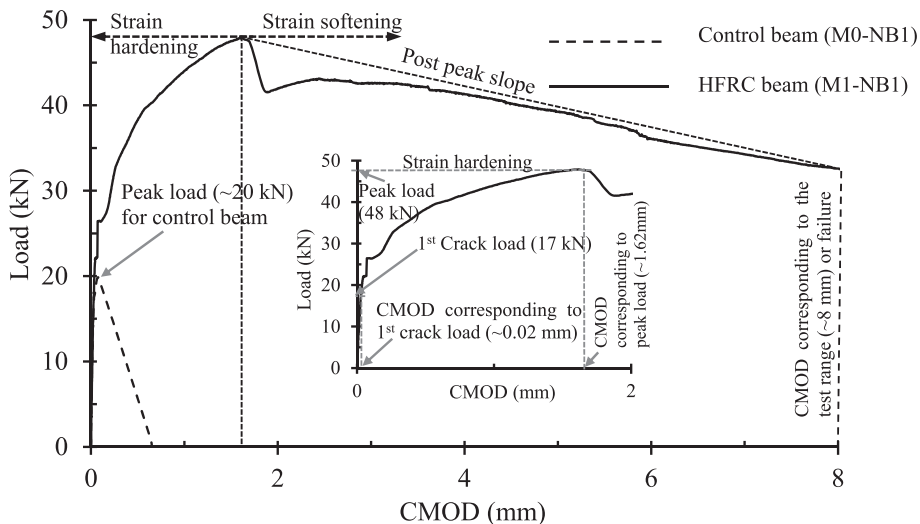


Fig. 4. Load-CMOD curves for control (M0-NB1) and HFRC composite beams (M1-NB1).

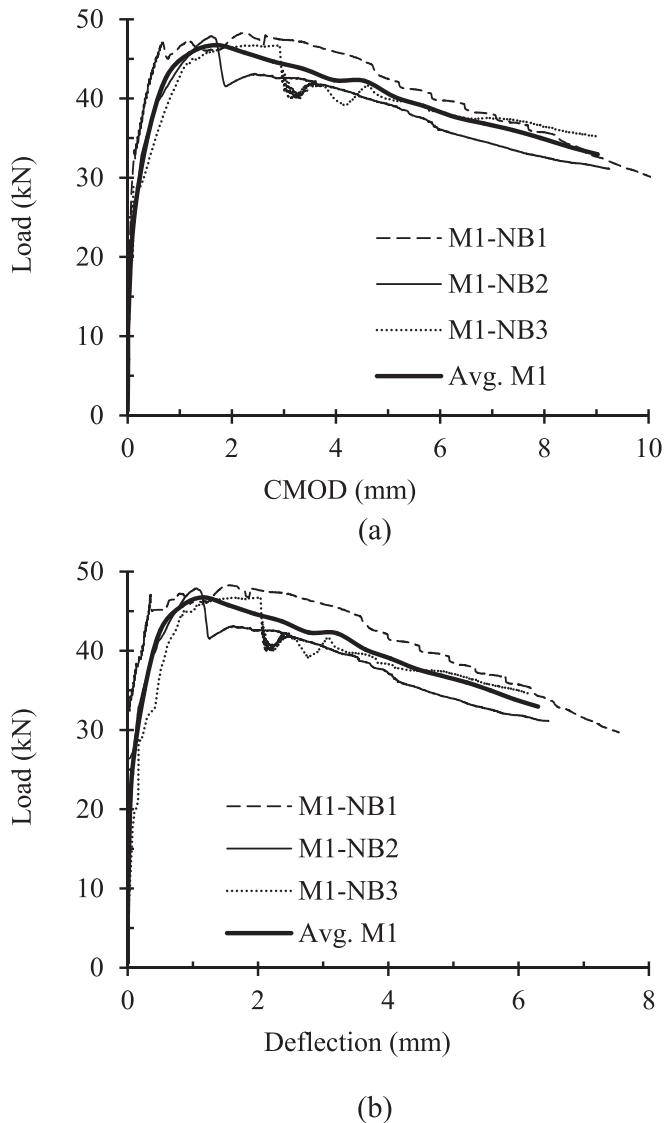


Fig. 5. Average curves for M1 beams: (a) Load-CMOD; (b) Load-Deflection.

beams due to the presence of fibers. The increase in the maximum load carrying capacity was in the range of 160% (M8 HFRC beam) to 240% (M4 HFRC beam). The load versus deflection/CMOD curves for HFRC composites also show a gradually descending branch.

The load-deflection/CMOD curves of HFRC composite beams illustrate hardening response followed by post peak softening. For HFRC composite beams, the slope of the load-deflection/CMOD curves remains same up to 55%–60% of the maximum load carrying capacity. The peaks correspond to the displacement values greater than 1 mm, except for the case of M7 beams, where the peak was observed at around 0.8 mm. With further increase in the loading, the strain softening behavior was observed in the descending branch. For the HFRC composites, the softening behavior can be characterized by linear decay with the negative slope ranging from 1.8 to 2.7 kN/mm (Table 5). Due to the high aspect ratio of fibers, the bond between matrix and fiber was strong and thus become the controlling criterion for arresting cracks. The average load-CMOD and load-deflection curves of HFRC composite beam specimen M1 are shown in Fig. 5.

M1 beams show minimum value of the average first crack load whereas the maximum value was observed for M7 beams. The

CMOD corresponding to the average first crack load was same (~0.02 mm) for all the tested beams. The average first crack load for HFRC composite specimens varies from 17.3 to 28.7 kN. For control beam, the average first crack load was 14.8 kN. The main reason for higher first crack loads for HFRC composite beams is due to the distribution of micro cracks over relatively large area because of the presence of fibers. Due to these micro cracks, the apparent change in the slope of the load versus CMOD curves of HFRC composites is quite small. The change in slope is visible only at the higher load levels where the crack size becomes almost comparable to that of the control concrete beams.

4.3. Comprehensive reinforcing index

The cracking behavior of HFRC is dependent on a number of factors such as the geometrical and mechanical properties of fibers, fiber volume fraction, as well as matrix properties [54–59]. The resisting forces that are produced in fibers during concrete fracture are the anchorage force provided by deformed geometry of fibers (hooked ends or crimped) and the mechanical bond stresses of straight portion of fibers.

Ezeldin and Balaguru [60] used the concept of fiber reinforcing index in defining the parameters for the stress-strain curves of FRC containing hooked end steel fibers. This was later extended by researchers [61,62] in the generation of complete stress-strain curves of FRC produced using crimped steel fibers. However, due to the use of the steel fibers alone in these studies [60–62], the concept of reinforcing index was extended to hybrid fibers for describing the quasi-static mechanical properties of FRC in later studies [27]. The reinforcing index, RI_v , was defined as [60]:

$$RI_v = \sum_i^n RI_{vi}, \quad (2)$$

where, suffix i is used for fiber type and RI_v is the comprehensive reinforcing index. The value of i taken in this study is 1 for steel fibers; 2 for polypropylene fibers and 3 for Kevlar fibers. RI_{vi} is the value of comprehensive reinforcing index, RI_v , for the i th material which has been updated from the earlier model [10,27] for incorporating the effect of tensile strength of fibers, thus giving:

$$RI_{vi} = v_{fi} \frac{k_i l_i}{d_i} \left(\frac{f_{ti}}{f_{ts}} \right)^a, \quad (3)$$

where, v_{fi} is the volume fraction of fibers; k_i is the bond factor of fibers; l_i is the length of fibers; d_i is the diameter (or equivalent diameter for non-circular sections) of fibers; f_{ti} and f_{ts} are the tensile strength of the material of i th fibers and steel fibers respectively. The values of bond factors, k_i , for hooked-end steel, crimped polypropylene and plain Kevlar fibers of this study are taken as 1, 1 and 0.1 respectively and the value of tension stiffness parameter, a , is taken as 0.5. Taking RI_v into consideration, the mechanical as well as the post cracking properties of HFRC composites can be obtained through regression analysis of the experimental data. The models based on the comprehensive reinforcing index for the determination of the mechanical and the post cracking properties of HFRC composites are obtained with the assumption that the fiber volume fraction at the notched section (i.e. section of least resistance where failure takes place) is equal to the supplied fiber dosage for the beam.

4.4. Fracture energy

The fracture energy is the fundamental property which

Table 6
Derived fracture properties.

Group	Mix/Beam specimen	Reinforcing index, R_{lv}	Fracture energy up to CMOD ₄ , G_f (N/mm)	Flexural tensile strength, f_{ft} (MPa)	Equiv. tensile strength (MPa)		Residual tensile strength (MPa)				Fracture energy G_f^I (N/mm)
					$f_{eq,2}$	$f_{eq,3}$	$f_{R,1-CMOD}$	$f_{R,2-CMOD}$	$f_{R,3-CMOD}$	$f_{R,4-CMOD}$	
Control	M0	0.00	0.107	5.1	—	—	—	—	—	—	0.28
Group-1	M1	1.07	8.02	13.7	17	18	11	13	13	13	39.94
	M2	1.02	8.53	14.2	15	21	12	13	14	13	37.82
Group-2	M3	1.25	9.87	17.1	26	26	14	17	16	15	48.35
	M4	1.20	10.31	17.4	22	24	15	16	16	15	45.44
Group-3	M5	0.84	8.13	13.4	17	18	12	13	13	13	35.10
	M6	1.02	8.57	14.6	23	21	13	14	13	12	37.14
Group-4	M7	0.97	9.22	15.7	15	20	15	15	14	13	39.57
	M8	0.79	7.78	13.3	16	17	12	13	12	11	28.53

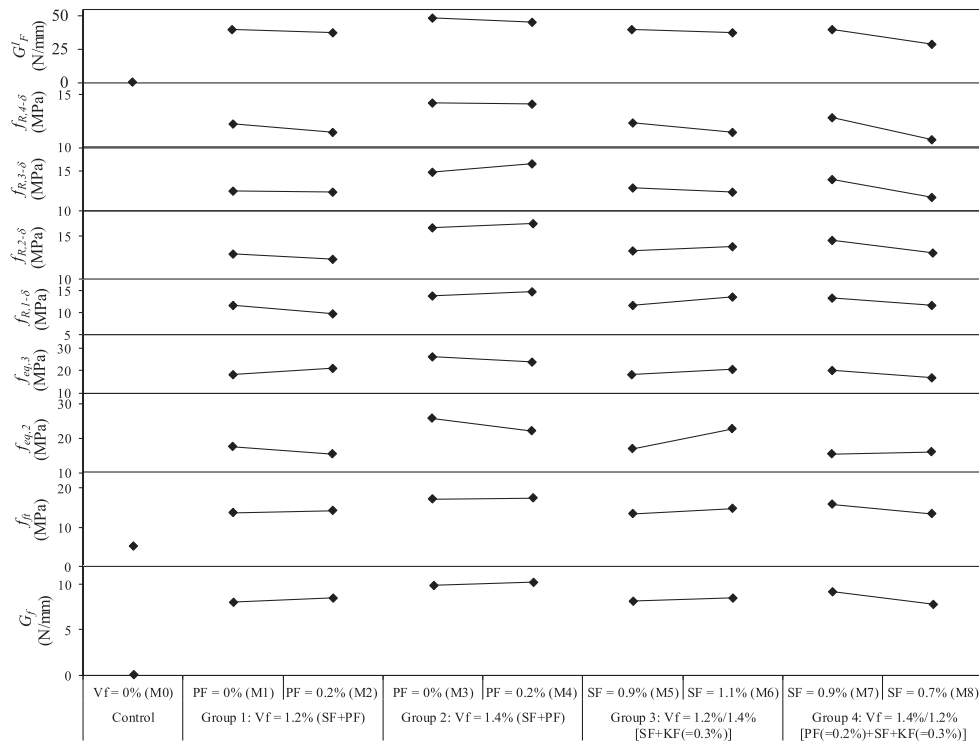


Fig. 6. Variation of fracture properties of HFRC composite beams.

determines the cracking resistance and fracture toughness of the material. The fracture energy, G_f , of the HFRC composite is calculated using the formula recommended by RILEM [63]:

$$G_f = \frac{W_o + mg\delta_f}{A_{lig}}; \tag{4}$$

where W_o is the area of the load-deflection curve; δ_f is the maximum displacement equivalent to 3.5 mm CMOD value; A_{lig} is the beam ligament area, calculated as $A_{lig} = bh_{eff}$, h_{eff} is the effective depth of the beam ($= h - a_o$), h and a_o are the depth of beam and notch depth respectively, mg is the weight of the beam spanning between the supports.

The fracture energies of different HFRC mixes are summarized in Table 6. The group-wise variation of fracture energy for the beams is plotted in Fig. 6. The following model has been developed (Fig. 7) for predicting the fracture energy, G_f , in terms of the reinforcing index, R_{lv} :

$$G_f = 4.4 R_{lv} + 4.3 \text{ (Units: N, mm)} \tag{5}$$

It is to be noted here that the above best fit line does not pass through the origin. It is thus valid for the range of R_{lv} for which it has been developed (i.e. $R_{lv} \geq 0.8$).

Because of the absence of any post-peak branch in the load-CMOD curves for control beams, the fracture energy of control was very small as a brittle failure was observed (Fig. 3). Compared to the control, the values of fracture energy of HFRC (i.e. M1 to M8) show an increase of two order of magnitude in the fracture energy of HFRC. This increase can be attributed to the cracking resistance due to the fiber bridging across the cracks [9], which primarily results in a large area covered by the descending branch of load-CMOD curve.

4.5. Flexural tensile strength

The flexural tensile strength of concrete is useful for determining the cracking resistance of the concrete materials. It has been

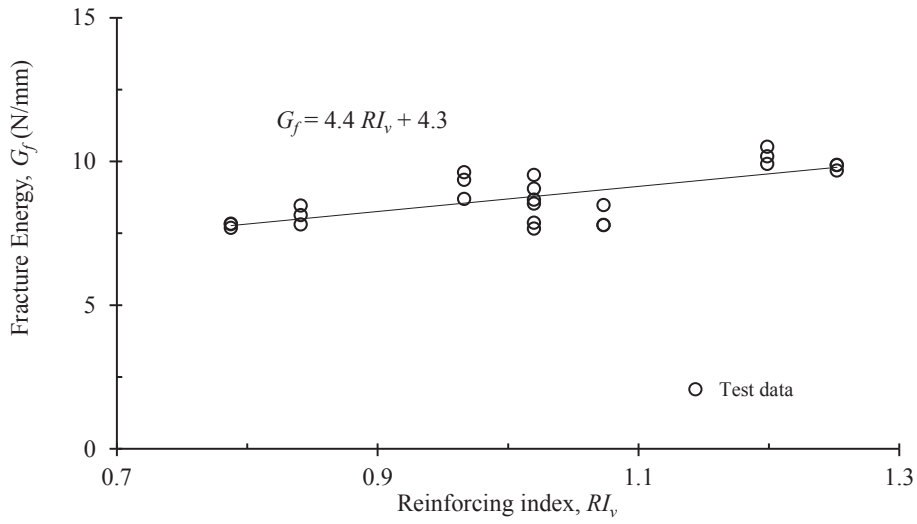


Fig. 7. Variation of fracture energy up to $CMOD_4$, G_f , with reinforcing index, R_{Iv} .

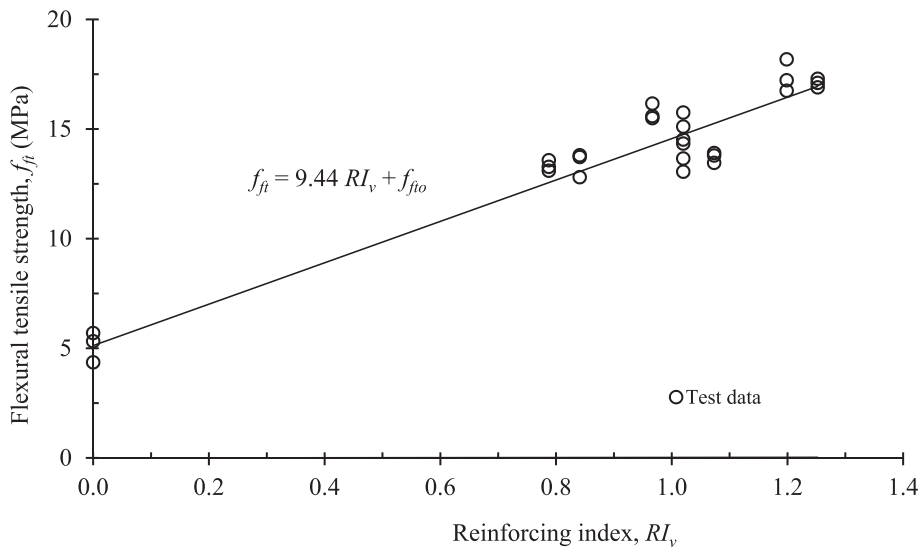


Fig. 8. Variation of flexural tensile strength, f_{ft} , with reinforcing index, R_{Iv} .

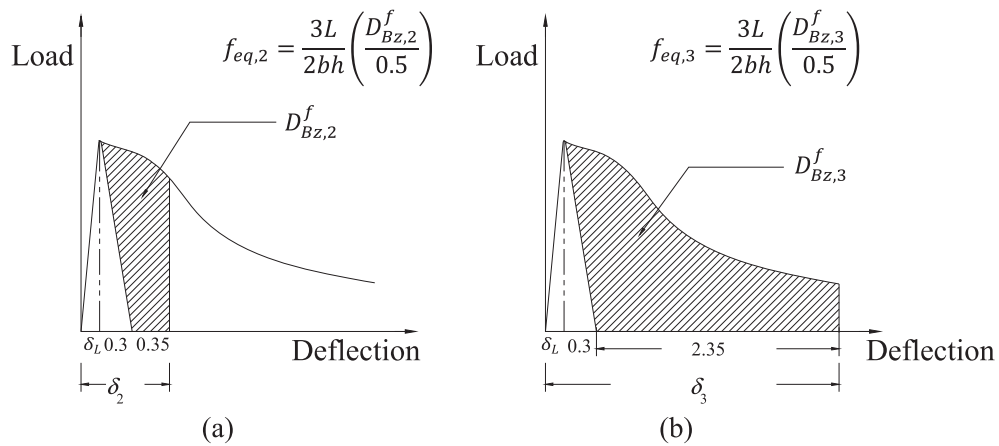


Fig. 9. Definition of equivalent tensile strengths: (a) $f_{eq,2}$; (b) $f_{eq,3}$ (δ_L = deflection corresponding to the highest value of load in the interval of 0–0.05 mm; $\delta_2 = \delta_L + 0.65$ mm; $\delta_3 = \delta_L + 2.65$ mm).

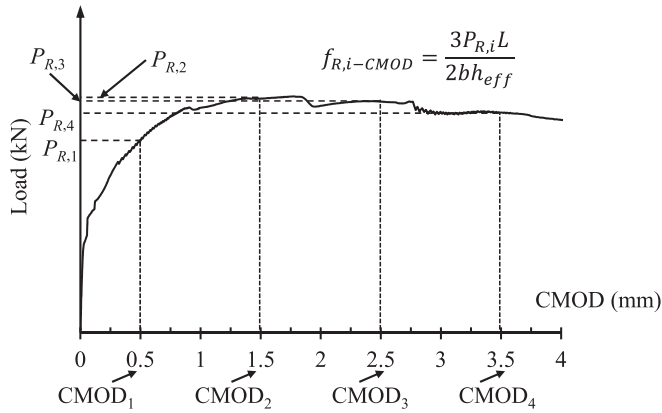


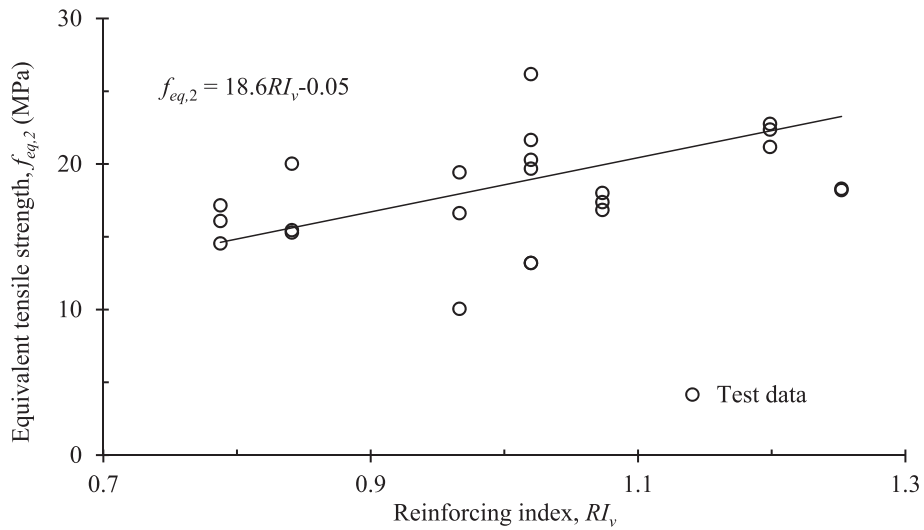
Fig. 10. Typical load-CMOD curve showing the standard values of CMOD used for the determination of residual tensile strength as recommended by RILEM [40] and fib Model Code2010 [64] (Note: Subscript *i* in the equation varies from 1 to 4).

used in this study for comparing the flexural response of different HFRC mixes. The flexural tensile strength of the concrete, f_{ft} , can be determined by using the following equation:

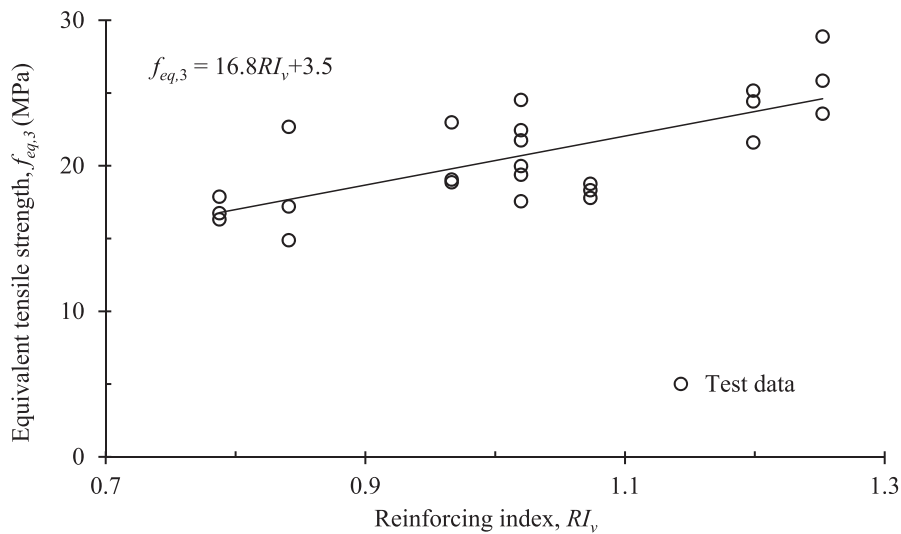
$$f_{ft} = \frac{3P_{max}L}{2b(h - a_o)^2} \tag{6}$$

where P_{max} is the maximum load and L is the effective span of the beam. The flexural tensile strengths for different HFRC composites are summarized in Table 6. The variation of flexural tensile strength is also plotted in Fig. 6. The addition of fibers in concrete results in two-fold increase (1.6–2.4) in the flexural tensile strength compared to the control. The variation of flexural tensile strength, f_{ft} , with the reinforcing index, RI_v is shown in Fig. 8. The model for the flexural tensile strength of HFRC composites can be given as:

$$f_{ft} = 9.44 RI_v + f_{fto} \text{ (Units: N, mm)} \tag{7}$$



(a)



(b)

Fig. 11. Variation of equivalent tensile strengths with reinforcing index, RI_v : (a) $f_{eq,2}$; (b) $f_{eq,3}$.

where f_{ft0} is the flexural tensile strength of plain concrete.

4.6. Equivalent and residual tensile strengths

In order to satisfy the serviceability limit states, the equivalent and the residual tensile strengths were calculated using the recommended procedure of RILEM [40] and fib Model Code2010 [64]. Fig. 9 shows the method of calculating the equivalent tensile strength of concrete for a typical load-deflection curve. The method is self-explanatory. The equivalent tensile strength represents the energy dissipated up to certain kinematic thresholds which gives an idea about the influence of fibers on the descending branch of the load-CMOD curves. The procedure of calculating the residual tensile strength of concrete for a typical load versus CMOD curve is summarized in Fig. 10. On the other hand, the residual tensile strength values provide an idea about the profile of descending branch of the load-CMOD curves. It may be noted that recent

guidelines [64] recommend the use of the residual tensile strength of FRC. However, previous studies [65] show that the residual tensile strength of FRC is relatively more susceptible to local irregularities of load-CMOD curves. Thus for the present study, both the equivalent tensile strength and the residual strength of FRC have been considered (Table 6). The group-wise variations of equivalent and residual tensile strengths are plotted in Fig. 6. The experimentally determined values of the second and third equivalent tensile strength as a function of reinforcing index, RI_v , are plotted in Fig. 11. Fig. 12 shows the variation of experimentally determined values of the residual tensile strengths as a function of reinforcing index, RI_v . The models given in Figs. 11 and 12 are valid for the range of RI_v for which these have been developed (i.e. $RI_v \geq 0.8$). It is observed from these figures that the second and third equivalent tensile strength and residual tensile strengths are increasing almost linearly with reinforcing index. It is worth mentioning here that the models given in these figures are

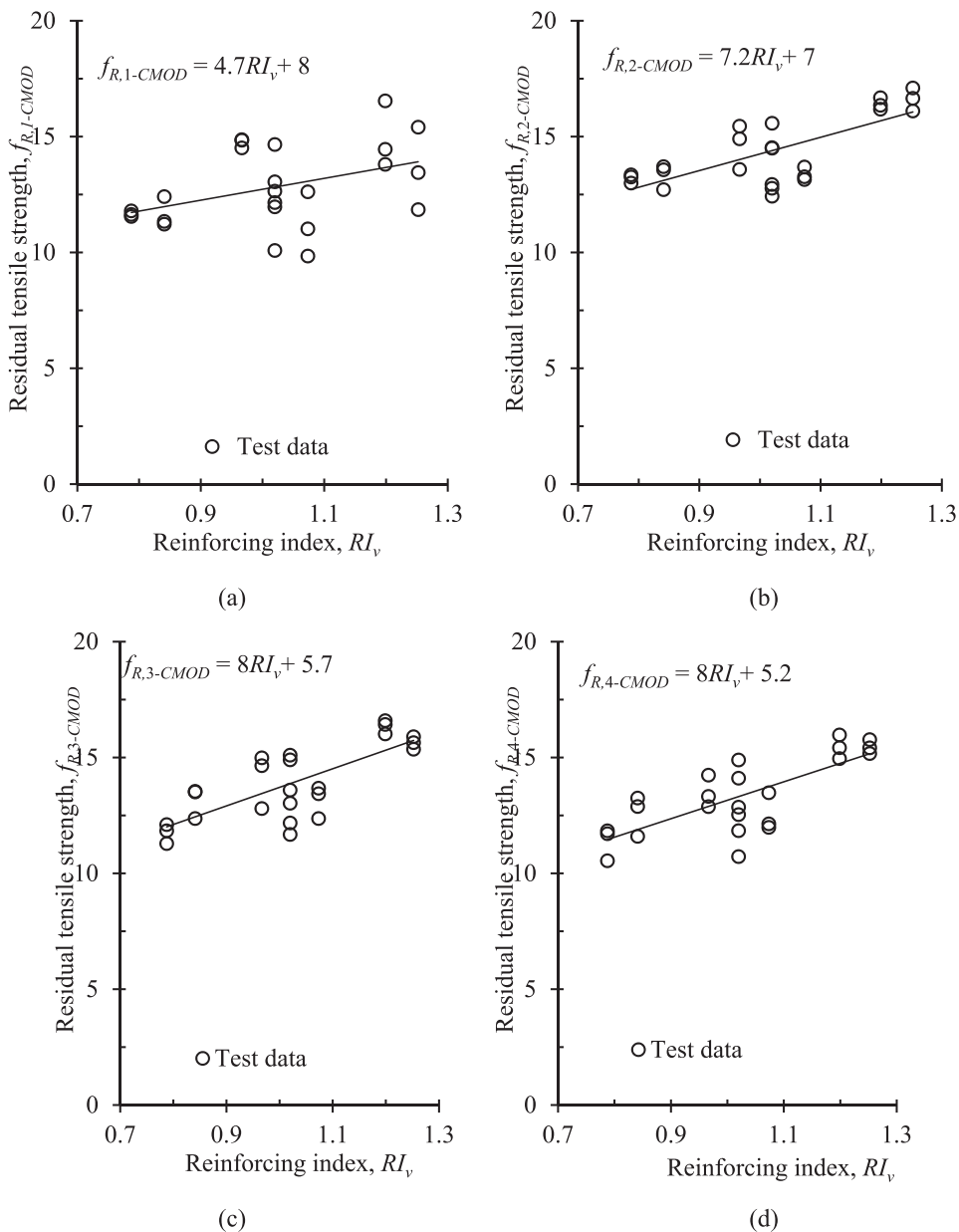


Fig. 12. Variation of residual tensile strengths (MPa) with reinforcing index, RI_v : (a) $f_{R,1-CMOD}$; (b) $f_{R,2-CMOD}$; (c) $f_{R,3-CMOD}$; (d) $f_{R,4-CMOD}$.

developed for the grade of concrete used in this study and its use for other concrete grades requires further verification.

4.7. Inverse analysis

In the present research, the tensile strength parameters of the HFRC beams are obtained using the multilayer inverse analysis procedure. Fig. 13 illustrates the principle involved in the analysis. The beam is cut in two equal halves, which are connected together by springs representing the stiffness of the notch section of HFRC. The beam depth at the notch in compression and tension zone is divided in n_1 and n_2 layers respectively. Different numbers of layers in compression and tension zones are used because of the adoption of the method of bi-section for the determination of neutral axis depth. Each spring represents the response of a layer at the notch section. The displacement variation at the notch section is assumed to be linear. The modulus of elasticity of HFRC in compression and tension is assumed to be same. The stress in each layer is determined from the stress–displacement relation of the springs which is represented by linear variation up to the peak stress followed by bi-linear post-peak behavior in tension thus leading to the four degrees of freedom system, as shown in Fig. 13. The maximum stress in compression is much less than the compressive strength of HFRC because of the tension failure of beams and thus the stress variation

in compression is linear (Fig. 13). The consideration of equilibrium of forces at the section gives:

$$\sum_{i=1}^{n_1} \sigma_{ci}b(\delta z_{ci}) + \sum_{j=1}^{n_2} \sigma_{tj}b(\delta z_{tj}) = 0 \tag{8}$$

where σ_{ci} = compressive stress in i th layer; σ_{tj} = tensile stress in j th layer; δz_{ci} , δz_{tj} = thickness of layers in compression and tension zones respectively. The external load, P , can be obtained from the equilibrium of moments at the section:

$$P = \frac{4}{L} \left[\sum_{i=1}^{n_1} \sigma_{ci}b(\delta z_{ci})z_i + \sum_{j=1}^{n_2} \sigma_{tj}b(\delta z_{tj})z_j \right] \tag{9}$$

where z_i , z_j = distance of the centroid of i th (compression) and j th (tension) layers respectively from top compression fiber of the beam.

The steps involved in the inverse analysis procedure are:

- i) Assume the parameters of tension strain-softening bi-linear curve. Although it involves assuming four parameters but for known tensile strength, it reduces to three parameters namely $f_{ct,aeq}$, w_c and w_o . The CMOD value, w_o , was taken as

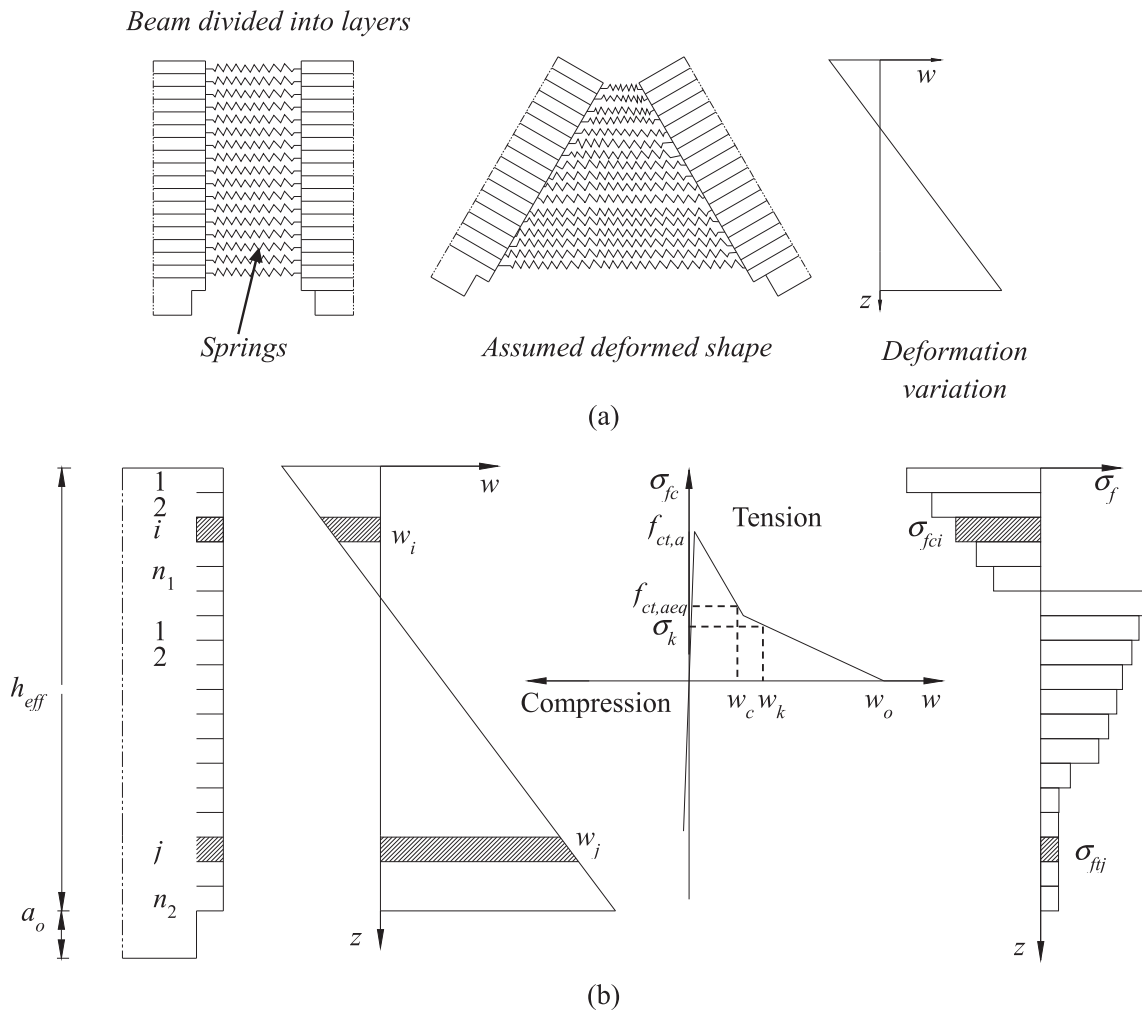


Fig. 13. Incremental procedure used in inverse analysis: (a) assumed springs and stress-deformation; (b) section analysis using slices.

half of the average fiber length [37]. The other two parameters were varied. The initial guess for these parameters was based on the shape of the experimental load-CMOD curve.

ii) Assume the depth of neutral axis. Its initial guess for the first load level was taken as $0.4h_{eff}$ and for the subsequent load

levels it was taken as the final converged value obtained for the previous load level.

iii) Assume a small CMOD value at the notch.

iv) Calculate displacements in different layers. Convert layer displacements to strains using the concept of fictitious length

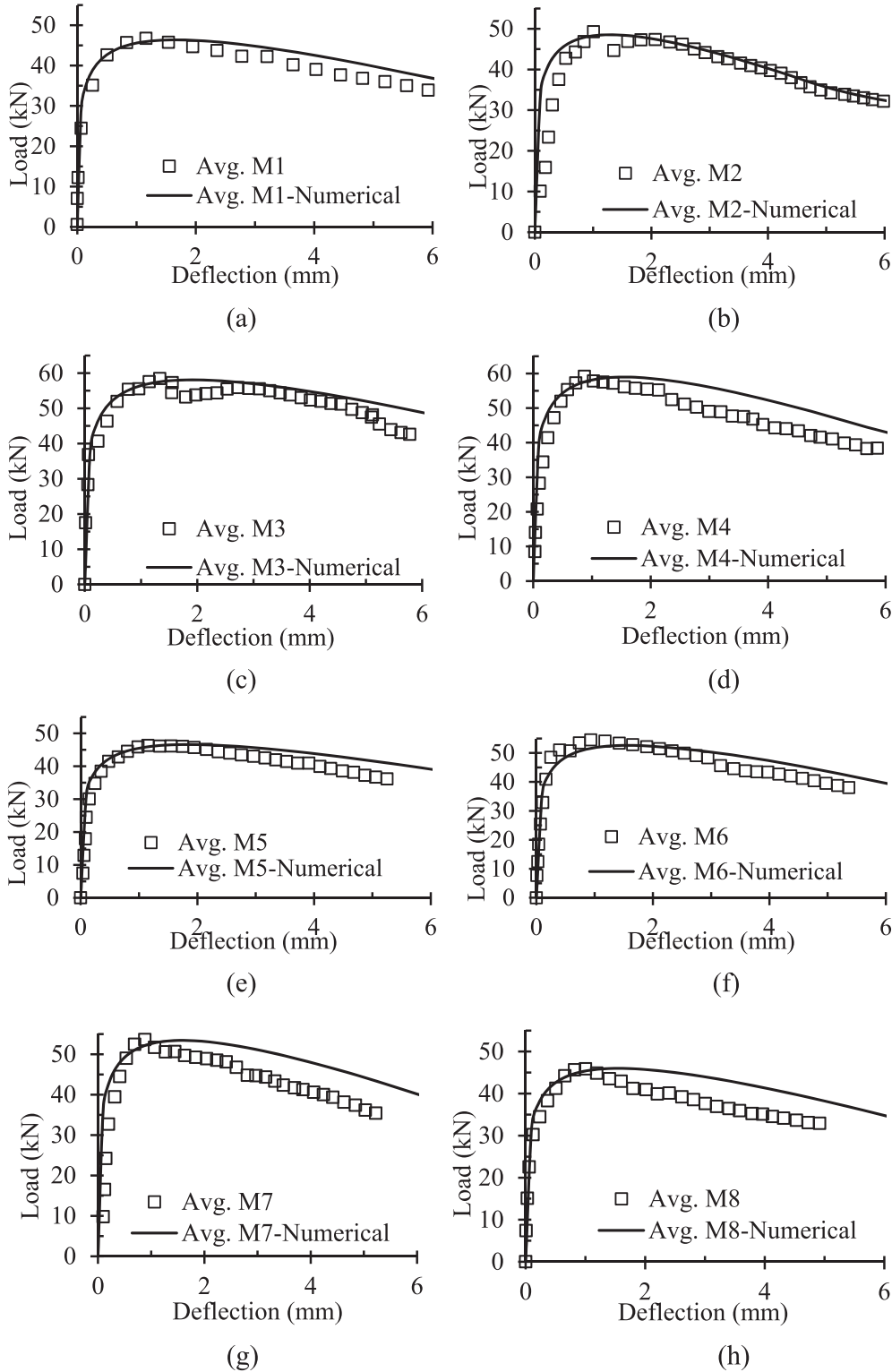


Fig. 14. Comparison between the experimental load deflection curve and the curve obtained using the inverse analysis for the HFRC composite beams: (a) M1; (b) M2; (c) M3; (d) M4; (e) M5; (f) M6; (g) M7; (h) M8.

[34]. The fictitious length of 125 mm was chosen for all the tested HFRC composite beams.

- v) Iterate on the depth of neutral axis for satisfying the equilibrium of forces i.e. Eq. (8).
- vi) Determine the magnitude of external load, P , using Eq. (9).
- vii) Increment CMOD and repeat from step (iv) for developing complete load-CMOD curve.
- viii) Match the analytical and experimental load-CMOD curves by adjusting the two parameters $f_{ct,aeq}$ and w_c and repeating from step (ii).

The analytical load-CMOD curves for beams obtained using the inverse analysis procedure along with their comparison with the

respective experimental load-CMOD curves are plotted in Fig. 14. The experimental load-CMOD curves of all HFRC mixes are also plotted together in Fig. 15. The values of the fracture energy obtained by the fitted parameters used for obtaining the analytical load-CMOD curves is given in Table 6. The variation of the fracture energy, G_F^I , along with the reinforcing index of different mixes is plotted in Fig. 16. The best-fit line gives a model for the prediction of fracture energy, G_F^I , of HFRC composite as:

$$G_F^I = 38.4RI_v + G_{F0}^I \quad (\text{Units : N, mm}) \quad (10)$$

where G_{F0}^I is the fracture energy of plain concrete (= 0.28 for mix M0).

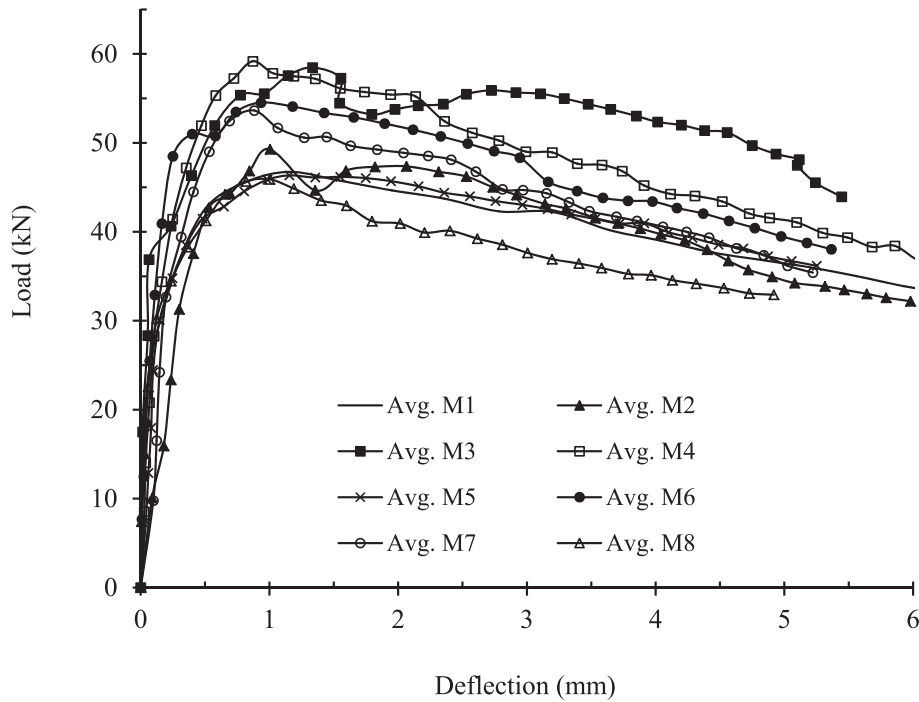


Fig. 15. Experimental load deflection curves of different HFRC mixes.

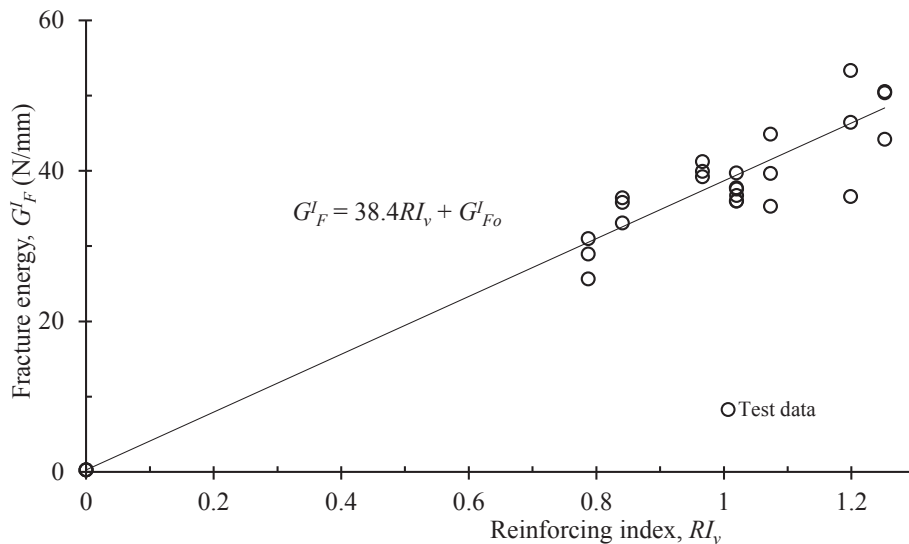


Fig. 16. Influence of fibers on the total fracture energy, G_F^I of HFRC composite beams.

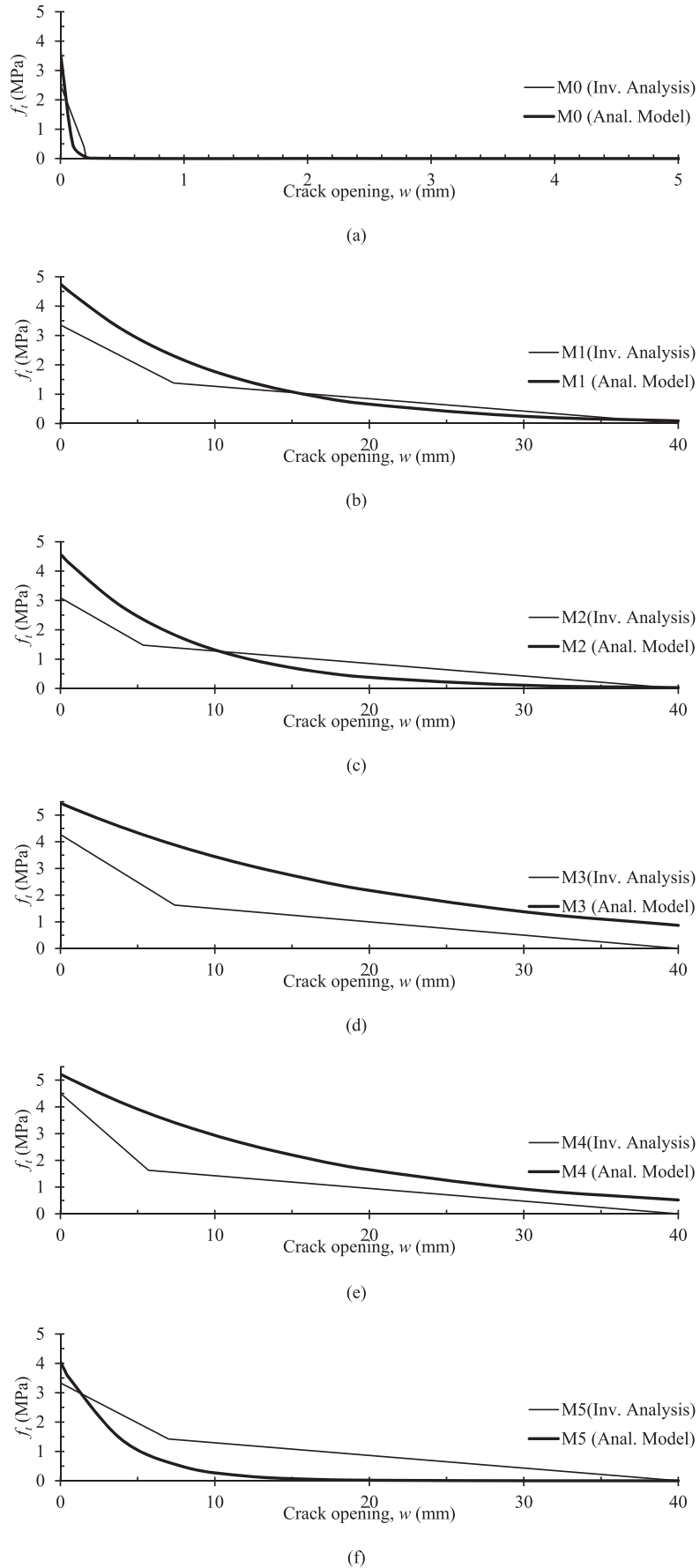


Fig. 17. Tensile softening diagram of HFRC composite beams: (a) M0; (b) M1; (c) M2; (d) M3; (e) M4; (f) M5; (g) M6; (h) M7; (i) M8.

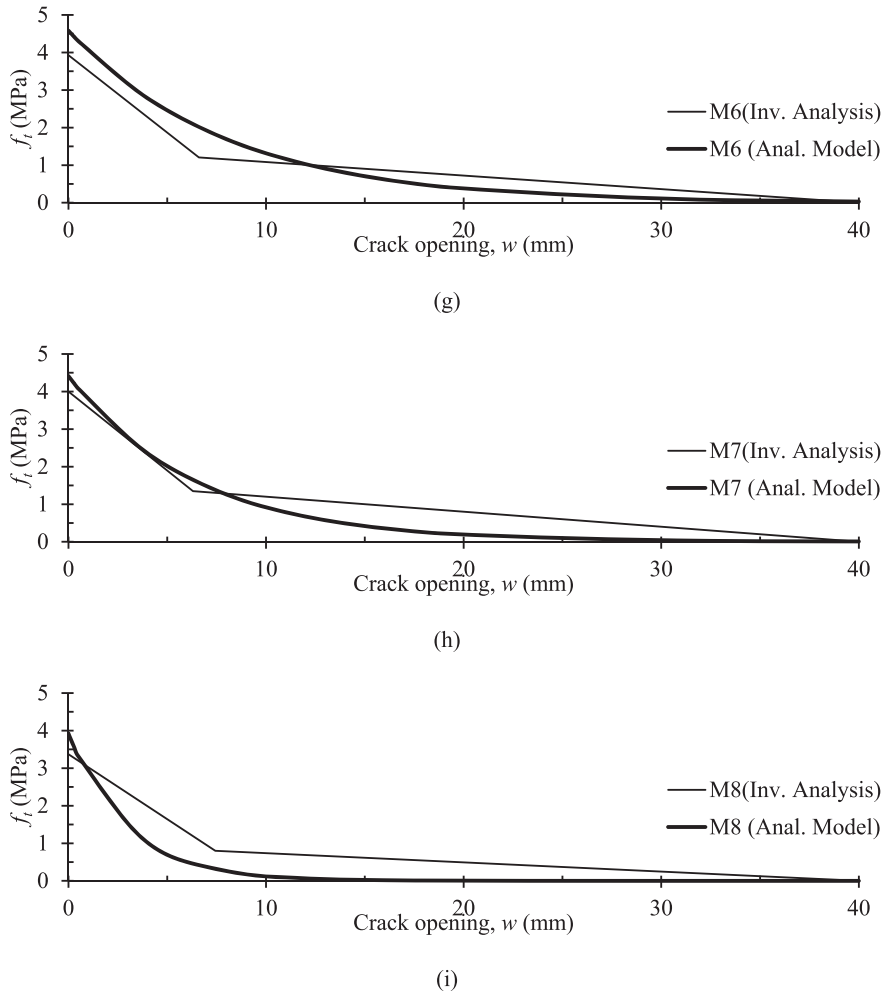


Fig. 17. (continued).

4.8. Discussions

Table 6 presents the fracture properties namely fracture energy (up to $CMOD_4$), flexural tensile strength, equivalent tensile strengths ($f_{eq,1}$ and $f_{eq,2}$), residual tensile strengths ($f_{R1,CMOD}$, $f_{R2,CMOD}$, $f_{R3,CMOD}$ and $f_{R4,CMOD}$) and the fracture energy of different HFRC mixes obtained directly from experiments and inverse analysis.

The influence of addition and/or replacement of different fibers on the fracture properties of HFRC mixes are discussed under three separate heads: (i) Effect of increase in SF fibers, (ii) Effect of replacement of SF fibers by PF fibers, and (iii) Effect of replacing SF fibers by KF fibers.

(i) **Effect of increase in SF fibers:** The influence of increase in the SF fiber fraction can be studied by comparing M1 with M3, M2 with M4, M5 with M6 and M7 with M8. The amount of increase in SF fiber volume in all these comparisons is 0.2%. As expected, these comparisons show that the increase in SF fiber volume results in 11%–45% increase in the fracture properties of HFRC mixes. The higher percentages are associated with the SF fibers alone because of better uniformity in the distribution of fibers.

(ii) **Effect of replacement of SF fibers by PF fibers:** A comparison of test results of M1 with M2, M3 with M4, M6 with M7 and M5 with M8 shows that partial replacement of 0.2%

volume of SF fibers by equal volume of PF fibers causes either no change or small increase (4%–16%) in the fracture properties of concrete (Table 6). Although the tensile strength of PF fibers is 45% of that of SF fibers, but the fracture strain of SF fibers is only 0.6% whereas the PF fibers fracture at 13.8% due to its low modulus. Thus PF fibers remain active even after the fracture or debonding of SF fibers which results in the improvement of fracture properties of concrete due to partial replacement of SF fibers by PF fibers.

(iii) **Effect of replacing SF fibers by KF fibers:** The effect of replacement of SF fibers by KF fibers can be studied by comparing M1 with M5, M3 with M6, M4 with M7 and M2 with M8. The replacement percentage in these comparisons is 0.3% by volume. A comparison shows that the replacement of SF fibers by KF fibers causes either almost no change or small decrease (2%–23%) in the values of fracture properties of HFRC. The higher decrease is mostly for the comparison of M3 with M6 in which the percentage of KF fibers is slightly higher (25% of total fiber volume) than in mix M5 (21.4% of total fiber volume). The reduction in fracture properties is mainly due to relatively inferior bond characteristics of KF fibers.

5. Analytical model for tensile softening diagram

For determining the tensile softening diagram of HFRC

composite, an analytical model based on the reinforcing index, RI_v , is also developed. The model is based on the extension of the existing model used for obtaining the tensile softening diagram for plain/SFRC [30]:

$$\sigma_c(w) = c_1 f'_{ct} e^{-c_2 w}; \quad (11)$$

where c_1 and c_2 are parameters influencing the peak strength and the steepness of the descending branch of concrete, respectively. f'_{ct} is a function of the tensile strength of concrete. The same expression (Eq. (11)) is used here to model the HFRC composite by incorporating the reinforcing index, RI_v , in the determination of model parameters. The model parameters used in the analytical model for tensile softening diagram can be expressed as:

$$c_1 = 0.75; \quad (12)$$

$$c_2 = \alpha e^{\beta RI_v}; \quad (13)$$

where the values of the model parameters α and β are 10 and -4.3 , respectively. The tensile strength of HFRC composite can be determined by using the following equation:

$$f'_{ct} = (f_{ct} - 1) + e^{\gamma RI_v}; \quad (14)$$

where f_{ct} is tensile strength of the control concrete. The value of γ in the above expression of f'_{ct} is 1.23.

Using the developed model given in Eq. (11), the tensile softening diagram for the different HFRC composites are plotted in Fig. 17 and compared with the experimental data obtained using the inverse analysis.

6. Conclusions

Experimental investigations on Mode-I fracture and post cracking behavior of HFRC composite have been carried out using the RILEM recommended three point bending test. The load versus crack mouth opening displacement (CMOD) curves of HFRC composite beams were obtained. Inverse analysis was also carried out. Influence of the different fibers used in the production of the HFRC composite on the post-cracking behavior of HFRC composite was investigated. Analytical models in terms of comprehensive reinforcing index were developed for determining the influence of the fibers on the fracture properties of HFRC composites. The following conclusions were drawn from the study:

- The increase in SF fiber volume results in increase in the fracture properties of HFRC mixes. The replacement of SF fibers by KF fibers causes either almost no change or small decrease in the values of fracture properties of HFRC. The replacement of SF fibers by equal volume of PF fibers causes either no change or small increase in the fracture properties of HFRC composites.
- Analytical models based on reinforcing index were developed for determining the fracture energy and flexural tensile strength which can be used for the mix design of HFRC composites.
- An analytical model is developed for predicting the tensile softening diagram of HFRC composite. The parameters required for the model are based on reinforcing index of hybrid fibers. The analytical model gives reasonable estimate of the tensile softening diagram of HFRC composites.

Acknowledgement

The project was supported by Deanship of Scientific Research Chairs at King Saud University, Saudi Arabia for the Chair of

Research and Studies in Strengthening and Rehabilitation of Structures at Civil Engineering Department.

References

- [1] M. Glavind, T. Aarre, High-strength concrete with increased fracture-toughness, Mater Res. Soc. Symp. Proc. 211 (1991) 39–46.
- [2] P. Soroushian, H. Elyamany, A. Tlili, K. Ostowari, Mixed-mode fracture properties of concrete reinforced with low volume fractions of steel and polypropylene fibers, Cem. Concr. Comp. 20 (1998) 67–78.
- [3] N. Banthia, M. Sappakittipakorn, Toughness enhancement in steel fiber reinforced concrete through fiber hybridization, Cem. Concr. Res. 37 (2007) 1366–1372.
- [4] N. Banthia, N. Nandakumar, Crack growth resistance of hybrid fiber reinforced composite, Cem. Concr. Comp. 25 (1) (2003) 3–9.
- [5] N. Banthia, F. Majdzadeh, J. Wu, V. Bindiganavile, Fiber synergy in hybrid fiber reinforced concrete (HyFRC) in flexure and direct shear, Cem. Concr. Comp. 48 (2014) 91–97.
- [6] H. Abbas, T. Almusallam, Y. Al-Salloum, Improving the impact resistance of reinforced concrete, Adv. Mater Res. 919–921 (2014) 1924–1929.
- [7] T.H. Almusallam, N.A. Siddiqui, R.A. Iqbal, H. Abbas, Response of hybrid-fiber reinforced concrete slabs to hard projectile impact, Int. J. Impact Eng. 58 (2013) 17–30.
- [8] T.H. Almusallam, A.A. Abadel, Y.A. Al-Salloum, N.A. Siddiqui, H. Abbas, Effectiveness of hybrid-fibers in improving the impact resistance of RC slabs, Int. J. Impact Eng. 81 (2015) 61–73.
- [9] I. Markovic, High-performance Hybrid-fibre Concrete: Development and Utilisation, PhD thesis, Delft University of Technology, The Netherlands, 2006.
- [10] S.M. Ibrahim, T.H. Almusallam, Y.A. Al-Salloum, A.A. Abadel, H. Abbas, Strain rate dependent behavior and modeling for compression response of hybrid fiber reinforced concrete, Lat. Am. J. Solids Struct. 13 (2016) 1695–1715.
- [11] T.N.S. Htut, Fracture Processes in Steel Fibre Reinforced Concrete, PhD Thesis, The University of New South Wales Australia, 2010.
- [12] P. Stahli, J.G.M. van Mier, Manufacturing, fibre anisotropy and fracture of hybrid fibre concrete, Eng. Fract. Mech. 74 (2007) 223–242.
- [13] M. Pajak, T. Ponikiewski, Flexural behavior of self-compacting concrete reinforced with different types of steel fibers, Constr. Build. Mater 47 (2013) 397–408.
- [14] N. Buratti, C. Mazzotti, M. Savoia, Post-cracking behaviour of steel and macro-synthetic fibre-reinforced concretes, Constr. Build. Mater 25 (2011) 2713–2722.
- [15] K.M.A. Hossain, M. Lachemi, M. Sammour, M. Sonebi, Strength and fracture energy characteristics of self-consolidating concrete incorporating polyvinyl alcohol, steel and hybrid fibres, Constr. Build. Mater 45 (2013) 20–29.
- [16] H. Cifuentes, F. García, O. Maeso, F. Medina, Influence of the properties of polypropylene fibres on the fracture behaviour of low-, normal- and high-strength FRC, Constr. Build. Mater 45 (2013) 130–137.
- [17] K. Watanabe, M.R. Bangi, T. Horiguchi, The effect of testing conditions (hot and residual) on fracture toughness of fiber reinforced high-strength concrete subjected to high temperatures, Cem. Concr. Res. 51 (2013) 6–13.
- [18] W. Sun, H. Chen, X. Luo, H. Qian, The effect of hybrid fibers and expansive agent on the shrinkage and permeability of high-performance concrete, Cem. Concr. Res. 31 (2001) 595–601.
- [19] N. Banthia, S.M. Soleimani, Flexural response of hybrid fiber reinforced cementitious composites, ACI Mater J. 102 (5) (2005) 382–389.
- [20] N. Banthia, R. Gupta, Hybrid fiber reinforced concrete: fiber synergy in high strength matrices, RILEM Mater Struct. 37 (274) (2004) 707–716.
- [21] C.X. Qian, P. Stroeven, Development of hybrid polypropylene-steel fiber reinforced concrete, Cem. Concr. Res. 30 (2000) 63–69.
- [22] N.W. Kim, N. Saeki, T. Horiguchi, Crack and strength properties of hybrid fiber reinforced concrete at early ages, Trans. Jpn. Concr. Inst. 21 (1999) 241–246.
- [23] J. Lawler, D. Zampini, S.P. Shah, Permeability of cracked hybrid fiber reinforced mortar under load, ACI Mater J. 99 (4) (2002) 379–385.
- [24] M. Fakhrafar, A. Dalvand, M. Arezoumandi, M.K. Sharbatdar, G. Chen, A. Kheyroddin, Mechanical properties of high performance fiber reinforced cementitious composites, Constr. Build. Mater 71 (2014) 510–520.
- [25] K.T. Soe, Y.X. Zhang, L.C. Zhang, Material properties of a new hybrid fibre-reinforced engineered cementitious composite, Constr. Build. Mater 43 (2013) 399–407.
- [26] M.G. Alberti, A. Enfedaque, J.C. Galvez, M.F. Canovas, I.R. Osorio, Polyolefin fiber-reinforced concrete enhanced with steel-hooked fibers in low proportions, Mater Des. 60 (2014) 57–65.
- [27] A. Abadel, H. Abbas, T. Almusallam, Y. Al-Salloum, N. Siddiqui, Experimental and analytical investigations of mechanical properties of hybrid fiber reinforced concrete, Mag. Concr. Res. 68 (16) (2016) 823–843.
- [28] J. Chen, N. Chouuw, Nonlinear flexural behaviour of flax FRP double tube confined coconut fibre reinforced concrete, Mater Des. 93 (2016) 247–254.
- [29] M.K. Lee, B.I.G. Barr, A four-exponential model to describe the behaviour of fibre reinforced concrete, Mater Struct. 37 (2004) 464–471.
- [30] A. Amin, S.J. Foster, A. Muttoni, Derivation of the σ - w relationship for SFRC from prism bending tests, Struct. Concr. (2015) 93–105.
- [31] E. Denneman, R. Wu, E.P. Kearsley, A.T. Visser, Discrete fracture in high performance fibre reinforced concrete materials, Eng. Fract. Mech. 78 (2011)

- 2235–2245.
- [32] J. Simo, J. Oliver, F. Armero, An analysis of strong discontinuities induced by strain-softening in rate-independent inelastic solids, *Comput. Mech.* 12 (5) (1993) 227–296.
- [33] D.S. Li, C. Hai, Q. Jinping, Fracture behavior and damage evaluation of poly-vinyl alcohol fiber concrete using acoustic emission technique, *Mater Des.* 40 (2012) 205–211.
- [34] D.A. Hordijk, Local Approach to Fatigue of Concrete, PhD thesis, Delft University of Technology, The Netherlands, 1991, pp. 131–134.
- [35] A.G. Kooiman, C. van der Veen, J.C. Walraven, Modelling the post-cracking behaviour of steel fibre reinforced concrete for structural design purposes, *HERON* 45 (4) (2000) 275–307.
- [36] J.F. Olesen, Fictitious crack propagation in fiber-reinforced concrete beams, *J. Eng. Mech.* 127 (3) (2001) 273–280.
- [37] T. Soetens, S. Mathys, Different methods to model the post-cracking behaviour of hooked-end steel fibre reinforced concrete, *Constr. Build. Mater* 73 (2014) 458–471.
- [38] N. Buratti, B. Ferracuti, M. Savoia, Concrete crack reduction in tunnel linings by steel fibre-reinforced concretes, *Constr. Build. Mater* 44 (2013) 249–259.
- [39] J. Zhang, C.K.Y. Leung, S. Xu, Evaluation of fracture parameters of concrete from bending test using inverse analysis approach, *Mater Struct.* 43 (2010) 857–874.
- [40] RILEM TC 162-TDF L. Vandewalle, et al., Test and design methods for steel fibre reinforced concrete – bending test, materials and structures, RILEM Publications, *Mater Struct.* 35 (2002) 579–582.
- [41] AASHTO T 177: Standard Method of Test for Flexural Strength of Concrete (Using Simple Beam with Center-point Loading). American Association of State Highway and Transportation Officials. Washington, USA.
- [42] ASTM C1550-12a Standard Test Method for Flexural Toughness of Fiber Reinforced Concrete (Using Centrally Loaded Round Panel), 2012. West Conshohocken, PA.
- [43] ASTM C1609/C1609M-12 Standard Test Method for Flexural Performance of Fiber-reinforced Concrete (Using Beam with Third-point Loading), 2012. West Conshohocken, PA.
- [44] ASTM C293/C293M – 15: Standard Test Method for Flexural Strength of Concrete (Using Simple Beam with Center-Point Loading), 2015. West Conshohocken, PA.
- [45] ASTM C78/C78M – 15: Standard Test Method for Flexural Strength of Concrete (Using Simple Beam with Third-Point Loading), 2015. West Conshohocken, PA.
- [46] DIN1048, Prüfverfahren für Beton; Teil 1: Frischbeton; Festbeton in Bauwerken und Bauteilen, DIN, 1991.
- [47] EFNARC, Specification for Sprayed Concrete, Final Draft Published by the European Federation of National Associations of Specialist Contractors and Material Suppliers to the Construction Industry (EFNARC), 1993, p. 35. Hampshire, UK.
- [48] EN 14651:2007 Test Method for Metallic Fibered Concrete – Measuring the Flexural Tensile Strength (Limit of Proportionality (LOP), Residual), European Standard, 2007.
- [49] JCI-S-001-2003 Method of Test for Fracture Energy of Concrete by Use of Notched Beam, Japan Concrete Institute Standard, 2003.
- [50] JCI-S-002-2003 Method of Test for Load-displacement Curve of Fiber Reinforced Concrete by Use of Notched Beam, Japan Concrete Institute Standard, 2003.
- [51] UNI-11039-2, Steel Fibre Reinforced Concrete – Test Method to Determine the First Crack Strength and Ductility Indexes, UNI Editions, Milan, Italy, 2003.
- [52] WSDOT Test Method No. 802 Method of Test for Flexural Strength of Concrete (Using Simple Beam with Center-Point Loading), Washington State Department of Transportation, 2009. WSDOT Materials Manual M 46–01.03.
- [53] ASTM C39/C39M-15a, Standard Test Method for Compressive Strength of Cylindrical Concrete Specimens, ASTM International, West Conshohocken, PA, 2015. www.astm.org.
- [54] N. Banthia, Study of some factors affecting the fibre-matrix bond in steel fibre reinforced concrete, *Can. J. Civ. Eng.* 17 (4) (1990) 10–620.
- [55] P. Guerrero, A.E. Naaman, Effect of mortar fineness and adhesive agents on pullout response of steel fibres, *ACI Mater J.* 97 (1) (2000) 12–20.
- [56] J.A. Mandel, S. Wei, S. Said, Studies of the properties of the fibre-matrix interfaced in steel fibre reinforced mortar, *ACI Mater J.* 84 (2) (1987) 101–109.
- [57] F. Laranjeira, C. Molins, A. Aguado, Predicting the pullout response of inclined hooked steel fibers, *Cem. Concr. Res.* 40 (2010) 1471–1487.
- [58] M.H.A. Beygi, M.T. Kazemi, I.M. Nikbin, J.V. Amiri, The effect of water to cement ratio on fracture parameters and brittleness of self-compacting concrete, *Mater Des.* 50 (2013) 267–276.
- [59] R. Madandoust, M.M. Ranjbar, R. Ghavidel, S.F. Shahabi, Assessment of factors influencing mechanical properties of steel fibre reinforced self-compacting concrete, *Mater Des.* 83 (2015) 284–294.
- [60] A.S. Ezeldin, P.N. Balaguru, Normal- and high-strength fiber-reinforced concrete under compression, *ASCE J. Mater Civ. Eng.* 4 (4) (1992) 415–429.
- [61] M.C. Nataraja, N. Dhang, A.P. Gupta, Stress-strain curves for steel-fiber reinforced concrete in compression, *Cem. Concr. Comp.* 21 (5–6) (1999) 383–390.
- [62] L. Taerwe, A. Gysel, Influence of steel fibers on design stress-strain curve for high-strength concrete, *J. Eng. Mech.* 122 (1996) 695–704.
- [63] RILEM FMC-50, Determination of the fracture energy of mortar and concrete by means of three point bend tests on notched beams, *Mater Struct.* 18 (4) (1985) 287–290.
- [64] fib MC2010 – International Federation for Structural Concrete, *fib Model Code for Concrete Structures* 2010, Verlag Ernst & Sohn, Berlin, 2013.
- [65] J.A.O. Barros, V.M.C.F. Cunha, A.F. Ribeiro, J.A.B. Antunes, Post-cracking behaviour of steel fibre reinforced concrete, *Mater Struct.* 38 (1) (2005) 47–56.